Dynamics of cascaded resonant radiations in a dispersion-varying optical fiber

A. Bendahmane, F. Braud, M. Conforti, B. Barviau, A. Mussot, A. Kudlinski

Dynamics of cascaded resonant radiations in a dispersion-varying optical fiber

A. Bendahmane, F. Braud, M. Conforti, B. Barviau, A. Mussot, A. Kudlinski

Dynamics of cascaded resonant radiations in a dispersion-varying optical fiber

A. BENDAHMANE[1], F. BRAUD[1], M. CONFORTI[1], B. BARVIAU[1,2], A. MUSSOT[1], AND A. KUDLINSKI[1,*]

[1] Laboratoire PhLAM UMR CNRS 8523, IRCICA USR CNRS 3380 Université Lille1, 59655 Villeneuve d'Ascq, France
[2] CORIA UMR CNRS 6614, Université de Rouen, 76801 Saint Etienne du Rouvray, France
[*] Corresponding author: alexandre.kudlinski@univ-lille1.fr

Compiled July 12, 2014

We use a dispersion-varying optical fiber to experimentally explore the dynamics of resonant radiations emitted from Raman-shifting solitons in the vicinity of the second zero-dispersion. The evolving zero-dispersion wavelength with fiber length allows to observe unprecedented processes such as a cascade of resonant radiations, the emission of multiple resonant radiations from a single soliton and the generation of a 500 nm continuum exclusively composed of resonant radiations. All experiments are interpreted using numerical simulations of the generalized nonlinear Schrödinger equation which are in excellent agreement.

OCIS codes: *(190.4370) Nonlinear optics, fibers; (190.5530) Pulse propagation and temporal solitons; (320.7140) Ultrafast processes in fibers.*

http://dx.doi.org/10.1364/optica.XX.XXXXXX

1. INTRODUCTION

Temporal solitons are fascinating localized structures in which dispersion is counterbalanced by nonlinearity [1]. In optical fibers, higher-order dispersion and/or nonlinear effects destabilize higher-order solitons which leads to their fission into fundamental ones [2], which are are much more robust and are only perturbed by these effects. An illustration of such a perturbation occurs when the soliton spectrum overlaps with the zero dispersion wavelength (ZDW) of the optical fiber [3]. In this situation, the soliton emits a resonant radiation (RR) (also termed dispersive wave or Cherenkov radiation) across the ZDW, mainly due to third-order dispersion [4]. The RR is generated at a higher (resp. lower) frequency than the the soliton if the third-order dispersion term is positive (resp. negative). This results in the spectral recoil of the soliton towards lower (resp. higher) frequencies as a consequence of the the momentum conservation of the process. The generation of RRs is usually explained in terms of phase-matching between the soliton and the RR [4]: $\beta_{RR}(\omega) = \beta_S(\omega)$, with β_{RR} the propagation constant of the RR and β_S the one of the soliton at the frequency of the RR. After a Taylor expansion of the propagation constants up to the third-order, this phase-matching relation becomes:

$$\frac{\beta_2}{2}\Omega^2 + \frac{\beta_3}{6}\Omega^3 = \frac{\gamma P}{2} \quad (1)$$

where β_2 and β_3 are the second and third-order dispersion terms, $\Omega = \omega_S - \omega_{RR}$ is the frequency separation between the soliton at ω_S and the RR at ω_{RR}, P is the soliton peak power and γ is the fiber nonlinear coefficient.

The emission of RRs from solitons has been largely investigated in uniform optical fibers, particularly in the context of supercontinuum generation [5]. The generation of RRs may also occur for a Raman shifting soliton when it reaches a second ZDW at long wavelengths [6]. In this case, the soliton self-frequency shift (SSFS) is cancelled because it is perfectly balanced by the spectral recoil due to the emission of a RR, which is red-shifted due to negative third-order dispersion [7]. Solitons and RRs may also interact and generate additional spectral components through nonlinear wave mixing processes dictated by a wave number matching condition, interpreted in terms of four-wave mixing (FWM) [8, 9]. Such interactions have been observed experimentally with ultrashort pulses [10, 11] and within the context of continuous-wave supercontinuum generation [12]. Recently the concept of RR has been extended to account for a new resonance with negative frequency part of the spectrum, that turns to be extremely blue-shifted [13]. Moreover it has been shown that the emission of RR is not a prerogative of solitons, but it can be shed by other sources such as shock waves [14, 15].

In axially-varying fibers, the generation of RRs may lead to even much more complex scenarios due to the design flexibility offered by these waveguides. The spectral recoil accompanying the emission of a RR may for instance lead to a soliton blue shift [16, 17, 18] as a result of the nonuniform fiber dispersion [17]. Recently, it has been shown with numerical simula-

tions that a single Raman shifting soliton can generate a polychromatic RR in a suitably engineered tapered fiber such that the ZDW remains close enough to the soliton spectrum along propagation [19]. Following the same idea, it has been shown numerically that multiple RRs can be generated from a single fundamental soliton in an axially segmented fiber by sequentially hitting the ZDW, which progressively shifts towards long wavelengths in order to follow the SSFS [20].

In this paper, we propose a detailed experimental and numerical study of the dynamics of RR generation in a dispersion-varying photonic crystal fiber (PCF) suitably tailored so that a Raman shifting soliton hits several times the long-wavelength second ZDW. This leads to a very rich and unprecedented dynamics in which (i) multiple RRs are emitted from a signal fundamental soliton (each time the soliton hits the ZDW), (ii) each generated RR, which remains temporally localized as a result of varying dispersion, cascades its own new RR and (iii) a continuum exclusively composed of RRs spanning over 500 nm is generated.

2. GENERATION OF CASCADED RESONANT RADIATIONS

We are interested here in a situation similar to the one described in [6], namely a soliton experiencing a Raman induced SSFS until it reaches the second ZDW where it stops and generates a RR across the ZDW. However, the important difference which is the key of our study is that the second ZDW evolves longitudinally so that the soliton or the RR hit it several times along propagation, which completely modifies the soliton/RR dynamics.

A. Fiber properties

Figure 1a (left axis) shows the evolution of the fiber diameter recorded during the drawing process. The initial uniform section is 7 m long and is such that the dispersion is anomalous over the 1000-1450 nm spectral range, a second ZDW being located at 1450 nm, as can be seen from Fig. 1a (solid line, right axis). This is achieved for a hole-to-hole spacing Λ of 1.17 μm and a relative hole diameter d/Λ of 0.64, with two bigger holes (d/Λ of 0.87) located apart from the core. This ensures a polarization maintaining behavior with an extinction ratio of about 20 dB over the spectral range of interest. The varying section has a cosine shape (starting from 7 m) and is obtained by varying the outer diameter during the fiber draw (Fig. 1a, left axis). This results in varying the hole-to-hole spacing while the relative hole diameter d/Λ is kept constant. The amplitude of oscillating section has been designed such that the ZDW decreases from 1450 nm (for the largest diameter) to 1140 nm (for the smallest one), as shown in Fig. 1a (solid line, right axis). The period of the oscillation has been fixed to 5 m, but it is worth noting that the periodic nature of the modulation does not play any role here (only the fact that the second ZDW alternatively increases and decreases is important). Full dispersion curves (simulated with a finite element mode solver) corresponding to the maximum and minimum diameters are plotted in Fig. 1b respectively in blue and red lines.

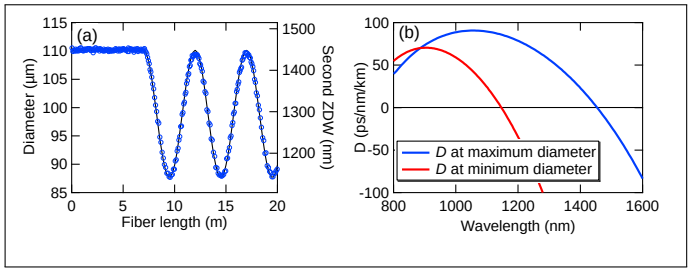

Fig. 1. a - Left axis: Evolution of the outer diameter of the dispersion-varying PCF versus length measured during the draw process (markers). Right axis: Simulated evolution of the second ZDW versus fiber length (solid line). b: Simulated dispersion curves for the maximum (blue line) and minimum (red line) fiber diameters.

B. Experimental setup

Figure 2 shows the experimental setup used for all experiments. The femtosecond oscillator delivers pulses centered at 1027.5 nm at a repetition rate of 54 MHz. After passing through an optical isolator, half-wave plates and a polarizer, they are launched into a 90/10 polarization maintaining coupler. At the coupler output (i.e. at the PCF input), the pulses have been fully characterized using a FROG system. They have a gaussian shape with a full-width at half maximum (FWHM) duration of 340 fs and the chirp parameter (defined as in [21]) is +1.5. The first half-wave plate HWF1 is used to adjust the input power and the second one, HWP2, allows to align the polarization state to a neutral axis of the coupler. The PCF is spliced to the 90 % output port of the coupler, with aligned neutral axes. The power was measured on the other output port which allows a very accurate and very reproducible control of the power launched in the PCF during cutback experiments presented hereafter.

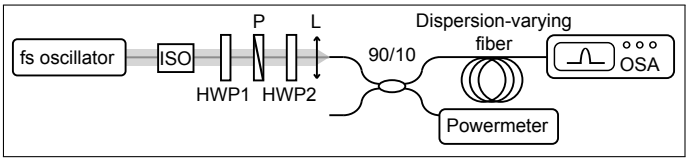

Fig. 2. Experimental setup. ISO: optical isolator, L: lens, HWP: half-wave plates, P: polarizer, OSA: optical spectrum analyzer.

C. Spectral domain analysis

In a first round of experiments, we investigated the dynamics of the spectrum with fiber length. This was done with a cutback procedure, in which the output spectrum is recorded after cutting back the PCF every 50 cm. Figure 3c shows the result of this experiment performed in the 20 m long PCF described in Fig. 1 for a pump power of 75 W effectively launched into the PCF (by taking into account the coupling rate of the coupler and splice loss). In this section, we firstly focus on the 12 m-long initial segment of the PCF (from 0 to the horizontal white dashed line in Fig. 3c). It is thus made of a 7 m long uniform section followed by a 5 m long section in which the diameter decreases and then increases again (see Fig. 1a). The processes occurring in the remaining of the fiber will be analyzed in the next section.

Figure 3b shows the output spectrum for the fiber length of 12 m. A soliton is ejected from the pump pulse and experiences Raman-induced SSFS. From 7 m, the SSFS increases because dispersion decreases [22], until it hits the decreasing ZDW (represented by the white line) at around 9 m. This results in the cancellation of the SSFS at 1120 nm and in the generation

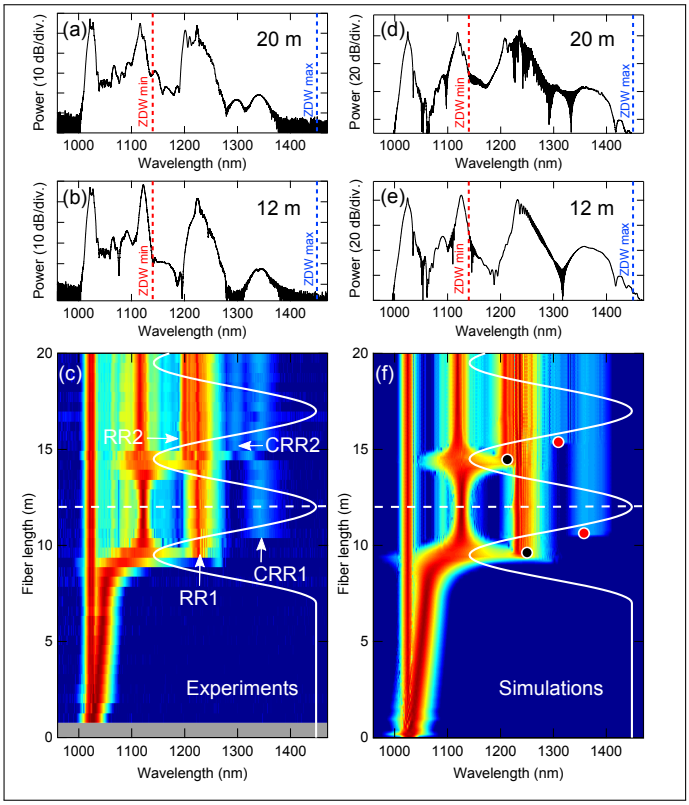

Fig. 3. a, d: Output spectrum after 20 m for a pump peak power of 75 W in (a) experiments and (d) simulations. b, e: Output spectrum after 12 m for a pump peak power of 75 W in (b) experiments and (e) simulations. Red and blue dashed lines represents respectively the minimum and maximum ZDW. c, f: Dynamics of the spectrum formation versus fiber length in (c) experiments and (f) simulations. The white solid line represents the second ZDW and the horizontal dashed line correspond the the fiber length of 12 m. Black and red dots represent phase-matched wavelengths of RR obtained with Eq. 1 from the soliton when it reaches the second ZDW and from the first generated RR when it crosses the ZDW, respectively.

of a RR (labeled RR1 in Fig. 3) around 1230 nm, as expected from [6]. This RR, initially located in normal dispersion, crosses the increasing ZDW (at 10.4 m). Simultaneously, an *a priori* unexpected spectral feature appears at even longer wavelengths around 1340 nm. Such features may originate from the nonlinear interaction of Raman-shifted solitons with RRs [8, 9, 10, 12] or with the residual pump radiation [23]. In the present case however, this additional feature appears 1 m after the RR generation, which suggest that another mechanism is involved in the generation process of the 1340 nm spectral feature.

In order to understand the physical origin of this feature, we performed numerical simulations of the generalized nonlinear Schrödinger equation (GNLSE) [21], taking into account the full dispersion curve as well as Kerr and Raman nonlinearities. The pump pulse used in simulations is the same as in experiments (340 fs gaussian pulse, +1.5 chirp parameter, 75 W peak power). The fiber parameters are the same as described above. Numerical simulations were thus performed without any adjustable parameter. The dynamics of the process obtained from numerical simulations displayed in Fig. 3f shows excellent agreement with experiments. In particular, the black dot located at 9 m in Fig. 3c represents the solution of the phase-matching relation (Eq. 1) for a soliton located at 1120 nm, in good agreement with simulations. Also, the appearance of the 1340 nm spectral feature is well reproduced, which allows us to study its physical origin more in details with help of numerical simulations in the time domain and numerical spectrograms.

D. Time domain analysis

In order to get further insight into this process, we numerically investigated the behavior of RR1 in the time domain. Figure 4 show the simulated time domain evolution along the fiber corresponding to the spectral one shown in Fig. 3f. As above, we focus our analysis here on the first 12 m of the fiber (the remaining section will be commented hereafter). Figure 3f shows that, quite surprisingly, RR1 remains localized in the time domain, on the contrary to usual RR1 observed in uniform fibers [6]. This is confirmed by the evolution of its peak power with fiber length, plotted in Fig. 4b, and by the temporal profiles of RR1 shown in the right column of Fig. 4 for various fiber lengths. When RR1 enters the anomalous dispersion region at 10.4 m, its peak power is of about 10 W. It then experiences a temporal compression so that its peak power increases from 6 W at 11 m (Fig. 4ϵ) to 36 W at 12.1 m (Fig. 4δ), as a result of the change in dispersion sign.

Having described spectral and temporal dynamics separately, we will now study their connections with help of numerical spectrograms.

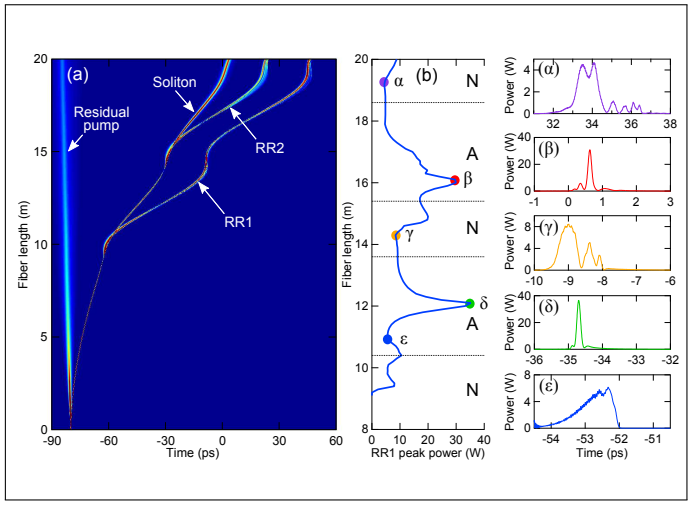

Fig. 4. a: Simulated time domain evolution (in linear scale) versus fiber length corresponding to Fig. 3f. b: Evolution of the peak power of RR1 with fiber length. Horizontal dotted lines depicts locations where the RR1 experiences a change in dispersion sign (N: normal dispersion; A: anomalous dispersion). α - ϵ: Simulated temporal profiles of RR1 at fiber lengths of 11, 12.1, 14.3, 16 and 18 m, respectively.

E. Spectro-temporal analysis

Figure 5b and c show the spectrograms corresponding to the simulation of Fig. 3f, for fiber lengths of 10.4 and 10.6 m respectively, just around the point where the RR hits the ZDW. At 10.4 m (Fig. 5a), the RR, which has previously been generated, is located in normal dispersion region and additional spectral components appear on both sides of the soliton/RR pair.

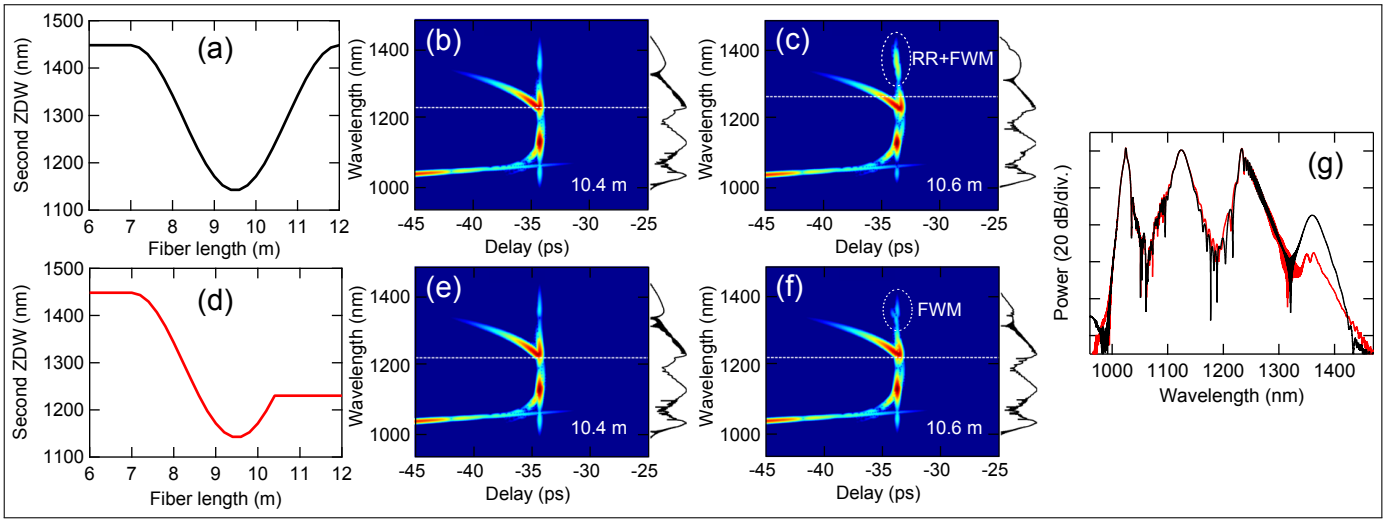

Fig. 5. Numerical spectrograms for fiber lengths of 10.4 and 10.6 m for the profiles displayed in a (top row) and d (bottom row) respectively. Horizontal white dashed lines depicts the second ZDW. g: Comparison between spectra obtained at 10.6 m in the profile of plot a (black line) and d (red line).

As we shall see hereafter, they originates from FWM between the soliton and the RR, as previously demonstrated in [8, 9]. At 10.6 m (Fig. 5c), the RR (labeled RR1 above) crosses the increasing ZDW (depicted by the white horizontal dashed line). This results in the generation of an additional radiation (around 1340 nm) across the ZDW, which can be seen as a new RR generation from the previous RR1 located at 1230 nm. Indeed, the red dot located at 10.4 m in Fig. 3f represents the solution of the phase-matching relation (Eq. 1) using RR1 as the solitonic pulse. Indeed, we demonstrate in the next section that RR1 actually contains a solitonic component. This whole process, that we name cascaded RR generation, is possible thanks to the high peak power of RR1 (Fig. 4b) when it crosses the ZDW, which is due to the dispersion-varying characteristics of the fiber. The spectral feature observed at 1340 nm thus originates both from FWM between the soliton and the RR and from the RR cascade because of the varying ZDW.

In order to confirm this, we performed numerical simulations in a fiber which has been designed so that the firstly generated RR does not cross the increasing ZDW (Fig. 5d). The ZDW has the same evolution as in Fig. 1a over the first 10.4 m, and it is then constant for the remaining of the fiber in order to cancel the change of dispersion sign experienced by the RR. In this case, the RR always remains in the normal dispersion region. Corresponding spectrograms are displayed in Figs. 5e and f for fiber lengths of 10.4 and 10.6 m respectively. The first one is identical to top row for a fiber length of 10.4 m, i.e. the first RR is generated and a FWM process between the soliton and the RR appears. For the length of 10.6 m (Fig. 5f), this time the RR does not cross the ZDW and the cascaded RR is not observed. Figure 5g shows a comparison between output spectra corresponding to these two cases (for the fiber profiles of Figs. 5a and d). The spectra looks very similar except around the 1340 nm radiation, which is much stronger in the fiber of Fig. 5a (real fiber). This is due to the fact that this peak (depicted by white dashed circles in Figs. 5c and f) is due to two different mechanisms in this case (FWM and cascaded RR), while only the FWM process happens in the fiber of Fig. 5d. In order to quantify the content of both processes to this spectral feature, it was numerically filtered and its energy was deduced by integrating the spectra of Fig. 5g. It is found that the 1340 nm peak of red curve in Fig. 5g (corresponding to the FWM process alone) represent only 0.6 % of the one of the black curve (corresponding to cascaded RR and FWM). This demonstrates that the cascaded RR process is largely predominant over the FWM one in our experiments.

These numerical results, supported by experiments, therefore provide evidence for a new process in which a soliton emits a RR which remains temporally localized thanks to the change of dispersion sign induced by the varying geometry along fiber. Thanks to this property, the RR has a high enough peak power to generate its own cascaded RR when it crosses the ZDW.

3. EMISSION OF MULTIPLE RESONANT RADIATIONS

In this section, we investigate the soliton/RR dynamics in a much more complex scenario when the Raman-shifted soliton hits the ZDW a second time, i.e. for a longer propagation distance. Therefore, we consider and analyze here the results of Figs. 3c and f over the remaining part of the fiber length, i.e. until 20 m.

A. Spectral analysis

Following the generation of the cascaded RR (labeled CRR1) around 1340 nm and according to the process described in section C, the soliton duration strongly increases because of the varying dispersion map, which is why it becomes spectrally compressed. It does not experience any significant SSFS at this point because of a too low peak power. When the ZDW decreases again from 12 m, the soliton temporally compresses so that its spectrum broadens and hits again the second ZDW around its minimum value at 14.5 m. This leads to the generation of a new RR (labeled RR2) located at a slightly different wavelength than RR1 because the soliton wavelength is slightly different at the point where it hits the ZDW. The black dot located at 14.5 m represents the solution of the phase-matching relation 1 for the corresponding soliton wavelength. It is in very good agreement with simulations, which confirms its origin. At 15 m, RR2 crosses the increasing ZDW which results in the generation of its own cascaded RR (labeled CRR2 in Fig. 3c),

following the same mechanism as described above. The red dot located around 15 m in Fig. 3f shows the solution of Eq. 1 with RR2 as solitonic pulse, in good agreement with the simulation result. Finally, after 20 m of propagation, the single fundamental soliton has directly generated two RRs, both of which have generated their own cascaded RR as observed in the output spectra of Figs. 3a and d (in experiments and simulations respectively).

B. Time domain analysis

The corresponding time domain map of Fig. 4a confirms that both RR1 and RR2 remains localized temporally, on the contrary to standard RRs generated in uniform fibers which rapidly spread out in time. In particular, Fig. 4b shows that the peak power of RR1 increases when it is located in anomalous dispersion region. In these regions and near the local maxima, RR1 is temporally compressed and its temporal profile resembles the one of a soliton (Figs. 4δ and β). On the contrary, in normal dispersion regions, RR1 tends to spread out in time and its shape is much more structured (Figs. 4γ and α) but it still have a peak power in the order of 10 W, which is enough to initiate the cascaded RR process. Cascaded RRs are not seen on Fig. 4a due to their reduced peak power as compared to RRs.

It can be demonstrated that, during the propagation in the anomalous dispersion regime, RR1 and RR2 contain solitons, showing unequivocally the nonlinear nature of these waves. To prove this fact, we solve numerically the direct Zakharov-Shabat (ZS) scattering problem [24] by means of the Fourier collocation method [25], for some profiles of RR1 at different fiber lengths. In doing this we neglect for the moment the Raman and higher-order dispersive effects and we take a constant value of the second order dispersion, evaluated at the corresponding fiber length. In this way, the GNLSE reduces to the integrable case, to which inverse scattering transform applies. The discrete spectrum of the ZS operator is associated to solitons, whereas the continuous spectrum gives linearly dispersing waves (radiation). The total energy of a given pulse is proportional the sum of two contributions: an integral over the continuous spectrum (radiation) and the sum of the imaginary parts of the discrete eigenvalues (solitons) of the ZS scattering problem [26]. We find that the field envelope of RR1 at $z = 12.1$ m (Fig. 4 δ) contains one soliton, that carries around 40% of the pulse energy, while at $z = 16$ m (Fig. 4 β) the pulse still contains one soliton that carries around 60% of the total energy. Similar results are found for RR2. The solitonic part contained in the RR is ultimately the source of the observed cascaded RR.

C. Spectro-temporal analysis

The video provided as supplementary material show the evolution of the simulated spectrogram centered on RR1 with fiber length. The horizontal dashed line represents the second ZDW. It confirms that RR1 remains temporally localized and shows how its overall chirp changes sign over successive dispersion regions. It also confirms the solitonic nature of RR1 discussed above at various locations along the fiber (around 12 and 16 m).

4. DYNAMICS OF POLYCHROMATIC RESONANT RADIATIONS EMISSION

Increasing the pump power results in a higher peak power of the first ejected soliton, and thus to a more efficient SSFS. As a consequence, the soliton hits the ZDW before its minimum value, i.e. when it is still decreasing. This situation is illustrated in Fig. 6 for a pump peak power of 110 W, where subfigures a and b correspond to experiments while c and d correspond to simulations. The soliton spectrum starts to overlap with the ZDW at about 9 m, i.e. at a point where it still decreases, and emits a RR. Then the soliton experiences a significant blue-shift [16, 17, 18] as a result of spectral recoil accompanying the RR emission combined with axially-varying dispersion [17]. Figure 7 shows a close-up on the RR emission observed around 9 m in Fig. 6d. The fiber ZDW (depicted by the white line) follows the blue-shifting soliton in such a way that its spectrum keeps overlapping with the normal dispersion region along propagation until about 10 m. This results in a continuous emission of RRs (or polychromatic RR) following the

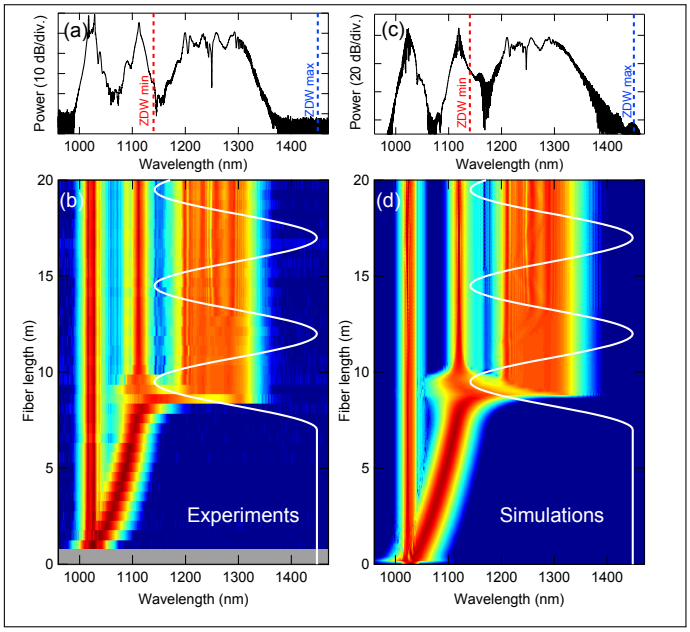

Fig. 6. a, c: Output spectrum after 20 m for a pump peak power of 110 W in (a) experiments and (c) simulations. b, d: Dynamics of the spectrum formation versus fiber length in (b) experiments and (d) simulations. The white line represents the second ZDW. Red and blue dashed lines in (a) and (c) represents respectively the minimum and maximum ZDW.

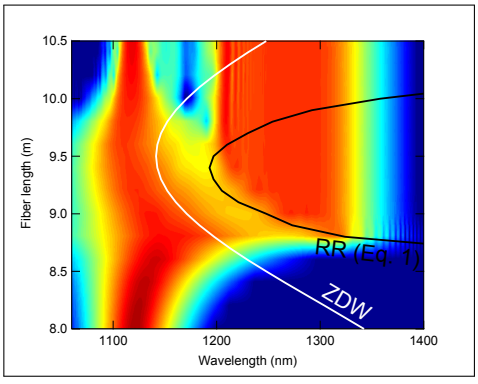

Fig. 7. Close-up on the RR emission observed around 9 m in Fig. 6d. The white line represents the second ZDW. The black line represents the phase-matching relation given by Eq. 1.

phase-matching relation 1 (depicted by the black line), similarly to the numerical results reported in Ref. [19]. In the simulation of Fig. 7, the soliton goes from 1145 nm at 8.8 m to 1115 nm at 9.4 m, which correspond to RRs located between 1325 nm and 1195 nm according to the phase-matching relation (black line), in excellent agreement with the simulated emission of RRs. This explains why RR spectrum is polychromatic and finally spans over more than 150 nm. After the emission of the polychromatic RR during its blue shift, the soliton does not have enough peak power left to experience SSFS again and hit again the ZDW. In our configuration, the emission of polychromatic RR is due to the fact that the soliton blue-shift follows the decreasing ZDW, while in Ref. [19] it is the SSFS which allows to follow the increasing ZDW.

The results of this section show how rich can be the dynamics of RR generation from a soliton in dispersion-varying optical fibers. They also provide the first experimental observation of polychromatic RRs predicted in Ref. [19].

5. GENERATION OF A RESONANT RADIATION CONTINUUM

In a last set of experiments, we studied the dynamics of RR generation in the case in which two solitons hit the fiber ZDW at different points. This is achieved by increasing the pump peak power to 380 W. Figure 8b shows the spectrum evolution with fiber length measured by successive cutbacks while Fig. 8d corresponds to numerical simulations. Experimentally, two main solitons are ejected from the break up of the pump pulse. The first one, labeled S1, has the highest peak power and shortest duration and therefore experiences the most important SSFS. It reaches the second ZDW in the uniform section of the fiber (after 4 m), so that it emits a RR (centered around 1550 nm) similarly to the case of Ref. [6]. As a consequence, the SSFS is cancelled and the soliton S1 keeps propagating until it hits the ZDW again when it starts to decrease from 7 m. This results in the generation of another RR centered at 1440 nm. The second soliton, labeled S2, has a less important SSFS rate than S1 due to its lower peak power and longer duration. It reaches the second ZDW at 8 m, at a point where the ZDW is decreasing. The soliton then disappears and transfers all its energy to a polychromatic RR. Finally, the output spectrum (displayed in Fig. 8a) is mainly composed of various RRs generated along the fiber, which makes a RR continuum between 1150 nm and 1650 nm. Simulations of Fig. 8d are in good agreement except the fact that the soliton S2 hits the second ZDW closer to its minimum value, possibly due to the presence of a nonlinear chirp on the pump pulse induced by the input coupler at this high pump power. As a consequence, the RR emitted by soliton S2 is less broad than in experiments, which results in a more structured RR continuum (Fig. 8c).

6. SUMMARY

We have investigated experimentally and numerically the generation of RRs from a soliton in the vicinity of the second ZDW of dispersion-varying optical fibers. Several major and unprecedented features have been identified. Firstly, we have observed and explained for the first time a process in which a RR radiated from a soliton emits itself a new cascaded RR when crossing the evolving ZDW of the fiber. Secondly, we have provided first experimental results showing the emission of multiple RRs from a unique soliton in a dispersion-varying optical fiber, following

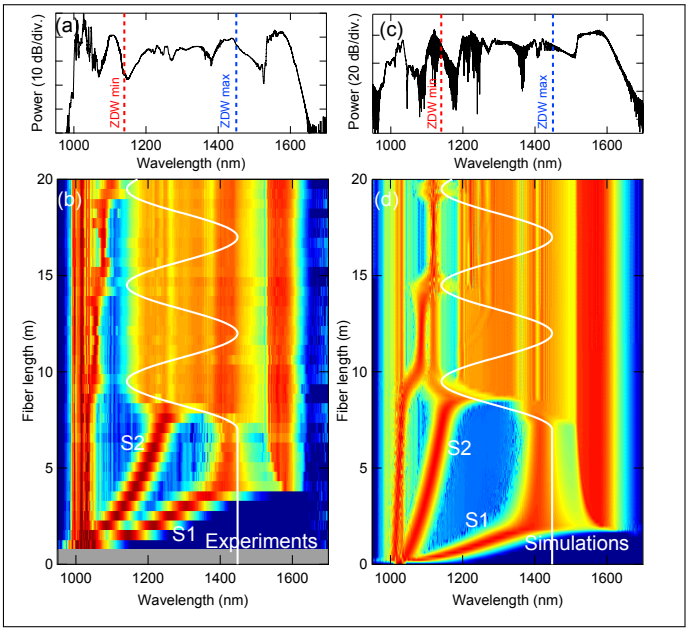

Fig. 8. a: Experimental output spectrum after 20 m for a pump peak power of 380 W. b: Measured dynamics of the spectrum formation versus fiber length. c: Simulated output spectrum. d: Simulated dynamics of the spectrum formation. The white line represents the second ZDW. Red and blue dashed lines in (a) and (c) represents respectively the minimum and maximum ZDW.

the numerical work from [20]. Thirdly, we have experimentally observed for the first time the generation of a polychromatic RR, as previously numerically investigated in [19], leading to a RR continuum spanning over 500 nm.

Our results show how the new degree of freedom brought by dispersion-varying optical fibers offers rich and complex dynamics of nonlinear effects and opens the door to a new way of thinking about nonlinear fiber optics.

FUNDING INFORMATION

This work was partly supported by the Agence Nationale de la Recherche through the ANR TOPWAVE project, by the French Ministry of Higher Education and Research, the Nord-Pas de Calais Regional Council and Fonds Européen de Développement Régional (FEDER) through the "Contrat de Projets Etat Région (CPER) 2007-2013" and the "Campus Intelligence Ambiante (CIA)".

REFERENCES

1. A. Hasegawa and M. Matsumoto, *Optical Solitons in Fibers* (Springer-Verlag Berlin and Heidelberg GmbH & Co. K, 2002).

2. P. Beaud, W. Hodel, B. Zysset, and H. Weber, "Ultrashort pulse propagation, pulse breakup, and fundamental soliton formation in a single-mode optical fiber," IEEE Journal of Quantum Electronics **23**, 1938–1946 (1987).

3. P. K. A. Wai, C. R. Menyuk, Y. C. Lee, and H. H. Chen, "Nonlinear pulse propagation in the neighborhood of the zero-dispersion wavelength of monomode optical fibers," Opt. Lett. **11**, 464–466 (1986).

4. N. Akhmediev and M. Karlsson, "Cherenkov radiation emitted by solitons in optical fibers," Phys. Rev. A **51**, 2602–2607 (1995).

5. J. M. Dudley, G. Genty, and S. Coen, "Supercontinuum generation in photonic crystal fiber," Rev. Mod. Phys. **78**, 1135–1184 (2006).

6. D. V. Skryabin, F. Luan, J. C. Knight, and P. S. J. Russell, "Soliton self-frequency shift cancellation in photonic crystal fibers," Science **301**, 1705–1708 (2003).

7. F. Biancalana, D. V. Skryabin, and A. V. Yulin, "Theory of the soliton self-frequency shift compensation by the resonant radiation in photonic crystal fibers," Physical Review E **70** (2004).

8. A. V. Yulin, D. V. Skryabin, and P. S. J. Russell, "Four-wave mixing of linear waves and solitons in fibers with higher-order dispersion," Opt. Lett. **29**, 2411–2413 (2004).

9. D. V. Skryabin and A. V. Yulin, "Theory of generation of new frequencies by mixing of solitons and dispersive waves in optical fibers," Phys. Rev. E **72**, 016619 (2005).

10. A. Efimov, A. Taylor, F. Omenetto, A. Yulin, N. Joly, F. Biancalana, D. Skryabin, J. Knight, and P. Russell, "Time-spectrally-resolved ultrafast nonlinear dynamics in small-core photonic crystal fibers: Experiment and modelling," Opt. Express **12**, 6498–6507 (2004).

11. A. Efimov, A. V. Yulin, D. V. Skryabin, J. C. Knight, N. Joly, F. G. Omenetto, A. J. Taylor, and P. Russell, "Interaction of an optical soliton with a dispersive wave," Phys. Rev. Lett. **95**, 213902 (2005).

12. B. H. Chapman, J. C. Travers, S. V. Popov, A. Mussot, and A. Kudlinski, "Long wavelength extension of CW-pumped supercontinuum through soliton-dispersive wave interactions," Opt. Express **18**, 24729–24734 (2010).

13. E. Rubino, J. McLenaghan, S. C. Kehr, F. Belgiorno, D. Townsend, S. Rohr, C. E. Kuklewicz, U. Leonhardt, F. König, and D. Faccio, "Negative-frequency resonant radiation," Phys. Rev. Lett. **108**, 253901 (2012).

14. K. E. Webb, Y. Q. Xu, M. Erkintalo, and S. G. Murdoch, "Generalized dispersive wave emission in nonlinear fiber optics," Opt. Lett. **38**, 151–153 (2013).

15. M. Conforti and S. Trillo, "Dispersive wave emission from wave breaking," Opt. Lett. **38**, 3815–3818 (2013).

16. Z. Chen, A. J. Taylor, and A. Efimov, "Coherent mid-infrared broadband continuum generation in non-uniform ZBLAN fiber taper," Opt. Express **17**, 5852–5860 (2009).

17. A. C. Judge, O. Bang, and C. Martijn de Sterke, "Theory of dispersive wave frequency shift via trapping by a soliton in an axially nonuniform optical fiber," J. Opt. Soc. Am. B **27**, 2195–2202 (2010).

18. S. P. Stark, A. Podlipensky, and P. S. J. Russell, "Soliton blueshift in tapered photonic crystal fibers," Phys. Rev. Lett. **106**, 083903 (2011).

19. C. Milián, A. Ferrando, and D. V. Skryabin, "Polychromatic cherenkov radiation and supercontinuum in tapered optical fibers," J. Opt. Soc. Am. B **29**, 589–593 (2012).

20. F. R. Arteaga-Sierra, C. Milián, I. Torres-Gómez, M. Torres-Cisneros, A. Ferrando, and A. Dávila, "Multi-peak-spectra generation with cherenkov radiation in a non-uniform single mode fiber," Opt. Express **22**, 2451–2458 (2014).

21. G. Agrawal, *Nonlinear Fiber Optics, Fifth Edition* (Academic Press, Amsterdam, 2012), 5th ed.

22. A. Bendahmane, O. Vanvincq, A. Mussot, and A. Kudlinski, "Control of the soliton self-frequency shift dynamics using topographic optical fibers," Opt. Lett. **38**, 3390–3393 (2013).

23. M. Erkintalo, J. M. Dudley, and G. Genty, "Pump-soliton nonlinear wave mixing in noise-driven fiber supercontinuum generation," Opt. Lett. **36**, 3870–3872 (2011).

24. V. E. Zakharov and A. B. Shabat, "Exact theory of two-dimensional self-focusing and onedimensional self-modulation of waves in nonlinear media," Sov. Phys. JETP **34**, 62–62 (1972).

25. J. Yang, *Nonlinear Waves in Integrable and Nonintegrable Systems* (SIAM, Philadelphia, 2012), 1st ed.

26. S. Burtsev, R. Camassa, and I. Timofeyev, "Numerical algorithms for the direct spectral transform with applications to nonlinear schrödinger type systems," J. Comput. Phys. **147**, 166–186 (1998).